THERMOHYDRODYNAMIC MODELING OF LASER CUTTING FOR RESIDUAL LASER ENERGY QUANTIFICATION USING A HYBRID LEVEL SET – MOVING MESH METHOD

R. MEILLOUR*'**, M. COURTOIS**, C. NAHED***, I. DOYEN*, M. CARIN**

**CEA, Service de Recherche en Matériaux et procédés Avancés, Université Paris – Saclay, Gif-sur-Yvette 91191, France*
***Université Bretagne Sud, UMR CNRS 6027, IRDL, Lorient 56100, France*
****CEA, Service d'Etudes Mécaniques et Thermiques, Université Paris – Saclay, Gif-sur-Yvette 91191, France*

DOI 10.3217/978-3-99161-089-2-018, license CC BY 4.0
https://creativecommons.org/licenses/by/4.0/deed.en
This CC license does not apply to third party material and content noted otherwise.

ABSTRACT

Although widely used and investigated in manufacturing, the laser cutting process remains an emerging technology for nuclear dismantling, where the challenges differ significantly. Indeed, while cutting quality is essential in manufacturing processes, it is not a relevant criterion in nuclear dismantling. Nevertheless, the residual laser energy, which is the focus of this study, is of particular relevance to nuclear safety issues for dismantling.

This paper presents a thermohydrodynamic model for simulating the laser cutting process of 5 mm thick 304L stainless steel, accounting for heat transfer and fluid flow in all phases (gas, liquid and solid), and employing the Level Set method to dynamically capture the gas-metal interface. The model is first validated through a comparison of the cutting front angles with experimental observations, demonstrating good agreement with a difference of less than 6%. The simulation results show good agreement with experimental observations regarding the cutting front angle, with a difference of less than 6%. Then, a hybrid Level Set – moving mesh method is proposed to discretize the interface in order to quantify the residual laser energy using the ray tracing approach.

Keywords: Laser cutting, heat and fluid flow, residual laser energy, Level Set, moving mesh, ray tracing.

INTRODUCTION

Since the first studies in the 1960s [1-2], the laser cutting process has been used across applications in various fields [3-6]. Among the industrial sectors involving the process, the

manufacturing industry is by far the most represented in the literature [7-9]. Indeed, in this sector the cutting quality, which is strongly affected by the formation of striations, remains a major weakness of the process. Most studies have investigated this phenomenon through both experimental [10] and numerical [11] analyses in order to eliminate striations.

In many numerical studies, both analytical and thermohydrodynamic models have been developed to describe physical mechanisms involved in laser cutting to predict the formation of striations as a function of operating parameters [12-13]. The thermohydrodynamic models provide a detailed representation of the process through the key physics such as heat transfer and fluid flow, as well as the gas – metal interface dynamic.

Both Amara *et al.* [14] and Kheloufi *et al.* [15] proposed thermohydrodynamic models for the laser cutting process on iron sheets (thickness $\leq 3\ mm$), relying on the Eulerian Volume Of Fluid (VOF) approach to capture the gas-metal interface and by solving the governing equations using the Finite Volume Method (FVM). Each thermohydrodynamic model [14-15] allows the investigation of the effect of certain operating parameters, such as the cutting velocity, on the kerf geometry and its temperature field, showing a good agreement with experimental work [16]. Amara *et al.* [13] extended their work with a more in-depth study that investigates the effect of laser wavelength on the cut quality, using a mesh adaption based on the temperature gradients to improve accuracy in regions of interest and reduce computational cost. More recently, Nie *et al.* [17] modeled the laser cutting of a $0.15\ mm$ aluminum alloy sheet, using a thermohydrodynamic approach and localized mesh refinement method as well. This study focused on particle ejection, highlighting mechanisms behind particle formation and characterizing their size and velocity post-ejection.

In nuclear application, challenges differ from those in the manufacturing industry. While cutting quality is a major interest in manufacturing, it is not a significant concern when dismantling nuclear facilities [18]. However, the portion of laser energy transmitted through the plate (Fig. 1), commonly referred to as residual laser energy, is largely overlooked in the literature, yet it requires particular attention in the context of nuclear safety issues for dismantling. Indeed, the residual laser energy could compromise the integrity of background structures due to its thermo-mechanical impact. The generation and dispersion of aerosols in the environment also present a challenge [19], however this aspect is not addressed in the present work.

This paper presents a 3D thermohydrodynamic model of laser cutting of a $5\ mm$ thick 304L stainless steel plate, including heat transfer and fluid flow equations for the three phases (gas, liquid and solid), as well as the Level Set method [20] to dynamically capture the gas-metal interface. A comparison with an experimental study [21] enables the first validation of the model by comparing cutting front angle, using the same operating parameters as those applied in the experiments. Then, a hybrid Level Set – moving mesh method coupled with a ray tracing approach is proposed to quantify the residual laser energy. The development of both the laser cutting model and the quantification of residual laser energy are carried out using the finite element software COMSOL Multiphysics®.

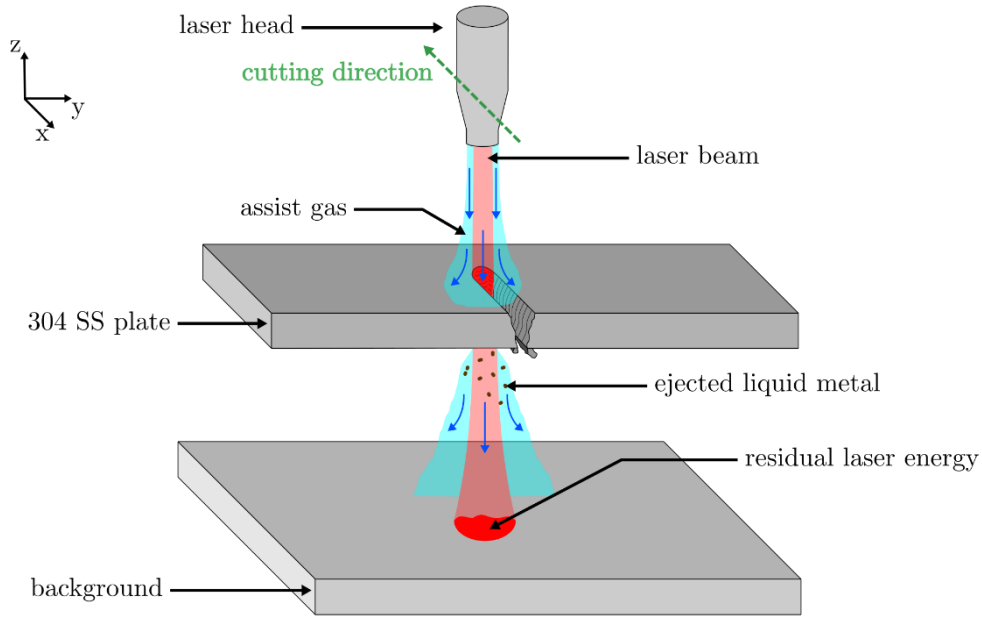

Fig. 1 Schematic view of the laser cutting process and the associated residual laser energy

MATHEMATICAL FORMAULATION OF THE LASER CUTTING MODEL

The present laser cutting modeling involves a multiphase and multiphysics approach. On the one hand, it must account for the gas, and metallic liquid and solid phases. On the other hand, it requires solving both heat transfer and fluid flow phenomena. Regarding these physics, the model is based on the following assumptions:

- Although Duan *et al.* [22] have shown that for plate thickness greater than 3 mm, multiple reflections of the laser within the kerf may influence the energy input into the plate, this phenomenon is not taken into account in this preliminary work.
- The process is modeled using an inert gas (nitrogen), and no chemical reactions are included.
- The properties of gas and metal (except for its thermal conductivity) are assumed constant with respect to temperature. A sensitivity analysis (not shown here) was performed on the thermophysical properties, which showed a limited impact on results.
- Given the complex nature of the hydrodynamics of the assist gas, it is not explicitly modeled, but rather represented by a friction force and a dynamic pressure, as proposed by Vicanek *et al.* [23].
- Based on the previous assumption, the flow is treated as laminar and the supersonic convective heat is not modeled.

Fig. 2 illustrates the thermohydrodynamic model used to simulate the laser cutting of a $5\,mm$ thick 304L stainless steel plate. The computational domain has dimensions of $6 \times 3.5 \times 7\ mm^3$. Owing to the symmetric nature of the process, the model includes only half of the cut, thus reducing the computational time. Although, in nuclear dismantling, the reference setup involves a static sample with a teleoperated or controlled laser head installed on a robotic arm, the model assumes a static laser cutting head while the plate moves along the x-axis at a cutting velocity $\overrightarrow{v_d}$. Indeed, this allows the computational domain to be reduced while preserving relevant information about the cutting front, thus lowering computational time.

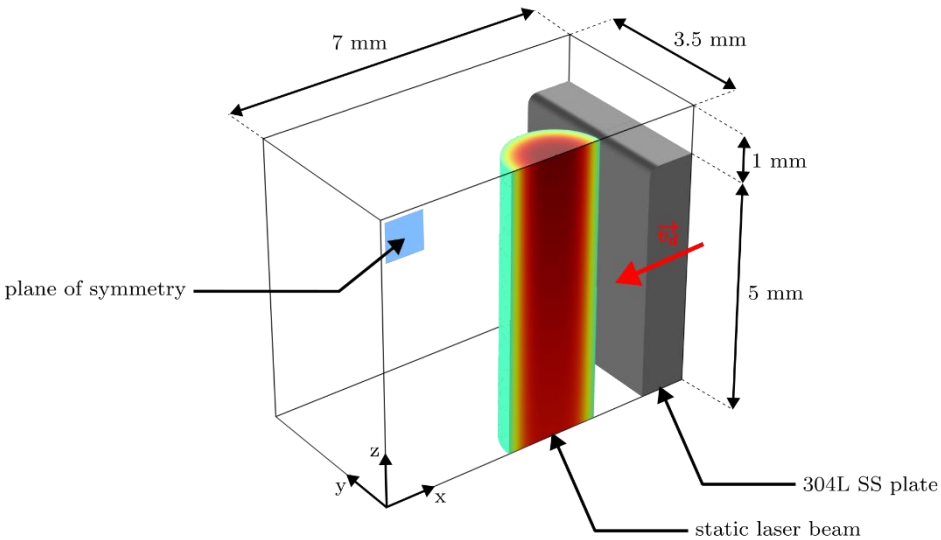

Fig. 2 Schematic representation of the thermohydrodynamic laser cutting model

GAS - METAL INTERFACE CAPTURING

The Level Set method, originally introduced by Osher and Sethian [20], is an Eulerian approach based on a fixed mesh and is employed in the model to dynamically capture the gas – metal interface, following the formulation of *Li et al.* [24]. The phase variable ϕ (refer to equation 1), which takes the value 0 in the gas phase and 1 in the metal phase (see Fig. 3), is determined by the following equation:

$$\frac{\partial \phi}{\partial t} + \vec{u} \cdot \vec{\nabla}\phi = \gamma_{LS}\, \vec{\nabla} \cdot \left[\varepsilon_{\mathrm{LS}}\, \vec{\nabla}\phi - \phi\,(1-\phi)\frac{\vec{\nabla}\phi}{|\vec{\nabla}\phi|} \right] \tag{1}$$

Where $\gamma_{LS}\ [m.s^{-1}]$ corresponds to the reinitialization parameter, and $\varepsilon_{\mathrm{LS}}\ [m]$ determines the thickness of the interface separating $\phi = 0$ and $\phi = 1$ phases in the Level Set formulation.

Here, the variable ϕ is advected by the velocity vector $\vec{u} = \{u, v, w\}$, as obtained from the Navier-Stokes equations (equations 14 and 15). Equation 2 presents $\delta(\phi)$, which is a smoothed approximation of the Dirac delta distribution. It enables the deposition of the physical phenomena occurring on the interface since no explicit boundary is defined. All properties are defined as a function of the variable ϕ, according to the formulation given in equation 3.

$$\delta(\phi) = 6\,|\phi(1-\phi)|\,\left|\vec{\nabla}\phi\right| \tag{2}$$

$$\xi = \xi_{gas} + \left(\xi_{metal} - \xi_{gas}\right)\phi \tag{3}$$

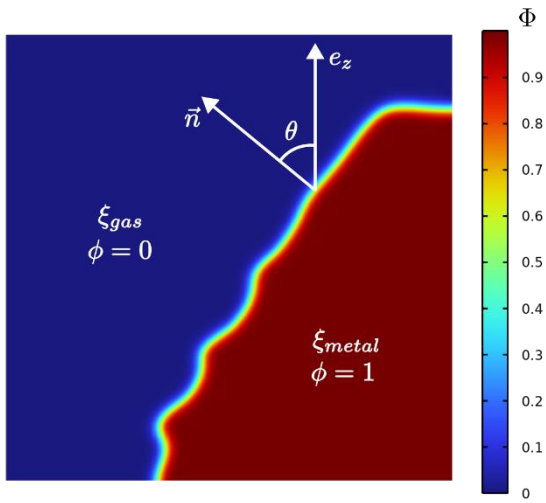

Fig. 3 Example of a 2D representation of the field $\boldsymbol{\phi}$

HEAT TRANSFER AND FLUID FLOW DESCRIPTIONS

The mathematical description of heat transfer, based on the previous assumptions, is computed by the thermal energy balance equation for isotropic and homogeneous materials (equation 4). The source terms include laser energy distribution S_{laser} (equation 5), and heat loses by vaporization S_{vap} (equation 10) and radiation S_{rad} (equation 13).

Here, the S_{laser} term accounts for the effect of the incidence angle θ (see figure 3) on the absorptivity α_{moy} through Fresnel's equations (equation 6 and 7) [25], the beam divergence from the focal plane position p_{fl} (equation 9), located 35 mm above the bottom surface of the plate, and a narrow Gaussian distribution due to the small diverging angle of the laser (6° [18]). S_{vap} is based on a modified Langmuir expression [26] and depends on the evaporated mass flux $\dot{m}$ $[kg.m^{-2}.s^{-1}]$ as a function of temperature T (equation 11). Considered of the second order, latent heat of fusion is omitted in the present model.

$$\rho_\phi \, c_{p_\phi} \left(\frac{\partial T}{\partial t} + \vec{u} \cdot \vec{\nabla} T \right) = \vec{\nabla} \cdot \left(\lambda_\phi \, \vec{\nabla} T \right) + \left(S_{laser} + S_{vap} + S_{rad} \right) \delta(\phi) \tag{4}$$

$$S_{laser} = \alpha_{moy}(\theta) \frac{P_{laser}}{\pi \, w(z)^2} \exp\left[- \left(\frac{({x_{laser}}^2 + {y_{laser}}^2)}{w(z)^2} \right)^2 \right] \cos\theta \tag{5}$$

$$\alpha_p(\theta) = 1 - \frac{(n^2 + k^2)\cos^2\theta - 2\,n\cos\theta + 1}{(n^2 + k^2)\cos^2\theta + 2\,n\cos\theta + 1} \tag{6}$$

$$\alpha_s(\theta) = 1 - \frac{(n^2 + k^2) - 2\,n\cos\theta + \cos^2\theta}{(n^2 + k^2) - 2\,n\cos\theta + \cos^2\theta} \tag{7}$$

$$\alpha_{moy}(\theta) = \frac{\alpha_p(\theta) + \alpha_s(\theta)}{2} \tag{8}$$

$$w(z) = w_0 \sqrt{1 + \left(\frac{z - p_{fl}}{z_R} \right)^2} \tag{9}$$

$$S_{vap} = -\dot{m} \, L_v \tag{10}$$

$$\dot{m} = (1 - \beta_r) \left(\frac{m}{2\,\pi \, k_B \, T} \right)^{\frac{1}{2}} p_{sat}(T) \tag{11}$$

$$p_{sat}(T) = p_0 \exp\left[\frac{\Delta H_v}{k_B \, T_{vap}} \left(1 - \frac{T_{vap}}{T} \right) \right] \tag{12}$$

$$S_{rad} = \varepsilon \, \sigma \, (T_{amb} - T)^4 \tag{13}$$

Where ρ is the density, c_p the heat capacity, λ the thermal conductivity, P_{laser} the laser power, n and k respectively the refraction index and the extinction coefficient, $w(z)$ the radius as a function of distance z and w_o the waist of the laser beam, x_{laser} and y_{laser} the coordinates of the laser, z_R the Rayleigh , β_R the retrodiffusion coefficient, m the atomic mass, k_B the Boltzmann constant, p_{sat} the saturation pressure of the vapor phase, the ambient pressure p_0 and temperature T_{amb}, L_v the latent heat of vaporization and ΔH_v the enthalpy of the phase transition (from liquid to vapor), T_{vap} the vaporization temperature, ε the emissivity and σ the Stephan-Boltzmann constant.

Table 1 summarizes the main parameters related to heat transfer, taken from experiments [21] and the literature [26,27-29]. Physical properties of 304L stainless steel are implemented in the model based on data available in the literature [27,29]. Given the absence of data for refractive index n and extinction coefficient k at the laser wavelength of $1030\ nm$ [21], values corresponding to iron at $1060\ nm$, as reported in [26], are employed.

Table 1 Summary of the main parameters used in heat transfer computation

Parameter [unit]	Value	Reference
λ_{304L} $[W.cm^{-1}.K^{-1}]$ solid / liquid	$8.116 \times 10^{-2} + 1.618 \times 10^{-4}\ T$ / $1.229 \times 10^{-3} + 3.248 \times 10^{-5}\ T$	[27]
ρ_{304L} $[kg.m^{-3}]$	7000	[29]
n / k	3.6 / 5	[28]
P_{laser} $[W]$	7000	[21]
w_0 $[\mu m]$	900	[21]
z_R $[mm]$	50	[18]
p_{fl} $[mm]$	35	[21]
L_v $[J.kg^{-1}]$	6.1 10^6	[26]
β_r	0.18	[26]
T_{vap} $[K]$	3134	[26]
ε	0.3	[29]

The fluid dynamics is described by the continuity equation (equation 14) and momentum conservation equations (equation 15) for laminar flow, considering both the gas and metal as incompressible and Newtonian fluids. The solid phase is modeled using a Darcy condition [30], which forces the solid velocity to tend toward the cutting velocity $v_{d\,x}$ along the x axis, and applying an augmented viscosity ($\mu_{solid} = 1\ Pa.s$) for temperature below the fusion temperature ($T_{fus} = 1700\ K$ [29]). The source terms $\overrightarrow{S_{fric}}$ and $\overrightarrow{S_{dyn}}$, which correspond to the friction force and dynamic pressure respectively, are introduced to account for the action of the assist gas on the molten metal [15,23]. The friction force is assumed to act as a tangential shear stress applied to the cutting front (xz-plane), leading to the neglect of the y-axis [15]. The surface tension effect $\overrightarrow{S_{st}}$ is also incorporated into the model, while its tangential force, known as the Marangoni effect, and the resulting temperature dependence of the surface tension coefficient γ are neglected.

$$\vec{\nabla} \cdot \vec{u} = 0 \tag{14}$$

$$\rho_\phi \left[\frac{\partial \vec{u}}{\partial t} + \left(\vec{u} \cdot \vec{\nabla}\right) \vec{u}\right] = \vec{\nabla} \cdot \left[-p\, I + \frac{1}{2}\, \mu_\phi \left(\left(\vec{\nabla}\, \vec{u}\right) + \left(\vec{\nabla}\, \vec{u}\right)^T\right)\right] + \rho_\phi\, \vec{g} \tag{15}$$

$$+\overrightarrow{S_{Darcy}} + \left(\overrightarrow{S_{fric}} + \overrightarrow{S_{dyn}} + \overrightarrow{S_{st}}\right) \delta(\phi)$$

$$\overrightarrow{S_{Darcy}} = \begin{cases} K\ (u + v_{d\,x}) \\ K\ v \\ K\ w \end{cases} \tag{16}$$

$$K = -C \left(\frac{(1 - f_l)^2}{{f_l}^3 + b}\right) \tag{17}$$

$$f_l = \begin{cases} 0 \; \forall \; T < T_s \\ \dfrac{T - T_s}{T_l - T_s} \; \forall \; T_s < T < T_l \\ 1 \; \forall \; T > T_l \end{cases} \tag{18}$$

$$\overrightarrow{S_{fric}} = \begin{cases} 2\sqrt{\dfrac{\rho_{gas}\,\mu_{gas}}{d}}\; {v_{AG}}^{\frac{3}{2}} \cos\theta \\ 0 \qquad\qquad\qquad \forall \; T < T_s \\ 2\sqrt{\dfrac{\rho_{gas}\,\mu_{gas}}{d}}\; {v_{AG}}^{\frac{3}{2}} \sin\theta \end{cases} \tag{19}$$

$$\overrightarrow{S_{dyn}} = \frac{1}{2}\,\rho_{gas}\,{v_{AG}}^2 \cdot e_z \quad \forall \; T < T_s \tag{20}$$

$$\overrightarrow{S_{st}} = \gamma\,\kappa\,\vec{n} \quad \forall \; T < T_s \tag{21}$$

Where T_s and T_l denote the solidus and liquidus temperatures, which are 1673 and 1727 K, respectively [29], μ the dynamic viscosity of the phase, $\vec{g}$ the gravitational acceleration vector, C and b the coefficients of the Darcy force, $v_{d\,x}$ the cutting velocity, f_l the liquid fraction, d the plate thickness, v_{AG} the assist gas velocity, e_z the unit vector along the z-axis, γ the surface tension coefficient, κ the curvature and $\vec{n}$ the normal vector of the gas-metal interface.

Table 2 Summary of the main parameters used in fluid flow computation

Parameter [unit]	Value	Reference
ρ_{304L} $[kg.m^{-3}]$	7000	[29]
μ_{304L} $[Pa.s]$ solid / liquid	1 / $4\;10^{-3}$	[29]
d $[mm]$	5	[21]
C / b	10^6 / 10^{-3}	[30]
T_s / T_l $[K]$	1673 / 1727	[29]
v_{AG} $[m.s^{-1}]$	943	[21]
γ $[N/m]$	0.15	[31]

SPATIAL AND TEMPORAL DISCRETIZATION

To reduce computational cost while maintaining an accurate representation of the cutting front, a multimesh approach is employed. Indeed, although the Level Set method requires a fine spatial discretization for the gas-metal interface and its interfacial phenomena, the fluid flow and, in particular, the heat transfer physics, do not require resolution using the same spatial discretization [30]. The multimesh approach is implemented using an identity mapping nonlocal coupling operator, as proposed by COMSOL Multiphysics®. The Level Set mesh

element size is fixed at $100\ \mu m$, with respective increases of 30 % and 40 % for the fluid flow and heat transfer meshes. Note that an excessive increase in the mesh size for either of these physics (fluid flow and heat transfer) may affect the accurate representation of the corresponding physical phenomena. The resolution using this spatial discretization represents 215 000 degrees of freedom (DOF). Regarding the spatial discretization, the time step is set to $20\ \mu s$.

RESULTS OF THE LASER CUTTING MODEL

The previously described mathematical formulation is used to simulate enables laser cutting process of a $5\ mm$-thick 304L stainless steel plate, with a laser power of $8\ kW$ and an assist gas flow rate of $400\ L.min^{-1}$ [21], corresponding to a velocity of $v_{AG} = 943\ m.s^{-1}$ at the nozzle output.

Fig. 4 presents the half kerf profile and the temperature field within the metallic phase for various cutting velocities. The final time step shown corresponds to a plate displacement of $-5\ mm$ along the x-axis. One can observe the influence of the cutting velocity on the kerf geometry, particularly on the cutting front and the sidewall angles. In this study, the focus is on the cutting front angle θ (Fig. 3), which is particularly relevant in relation to the residual laser energy and the experimental validation of the model [21]. Ideally, when the physical phenomena are accurately captured according to the operating parameters, the cutting front angles should closely match the experimental results.

Fig. 4 shows that higher temperatures, especially at the lower part of the cutting front, are reached at the highest cutting velocity ($24\ m.s^{-1}$). A possible explanation is the longer interaction time between the ejected liquid metal and the laser beam along the cutting front. Furthermore, these simulations also provide information regarding the fluid dynamics, such as the velocity magnitude (Fig. 4).

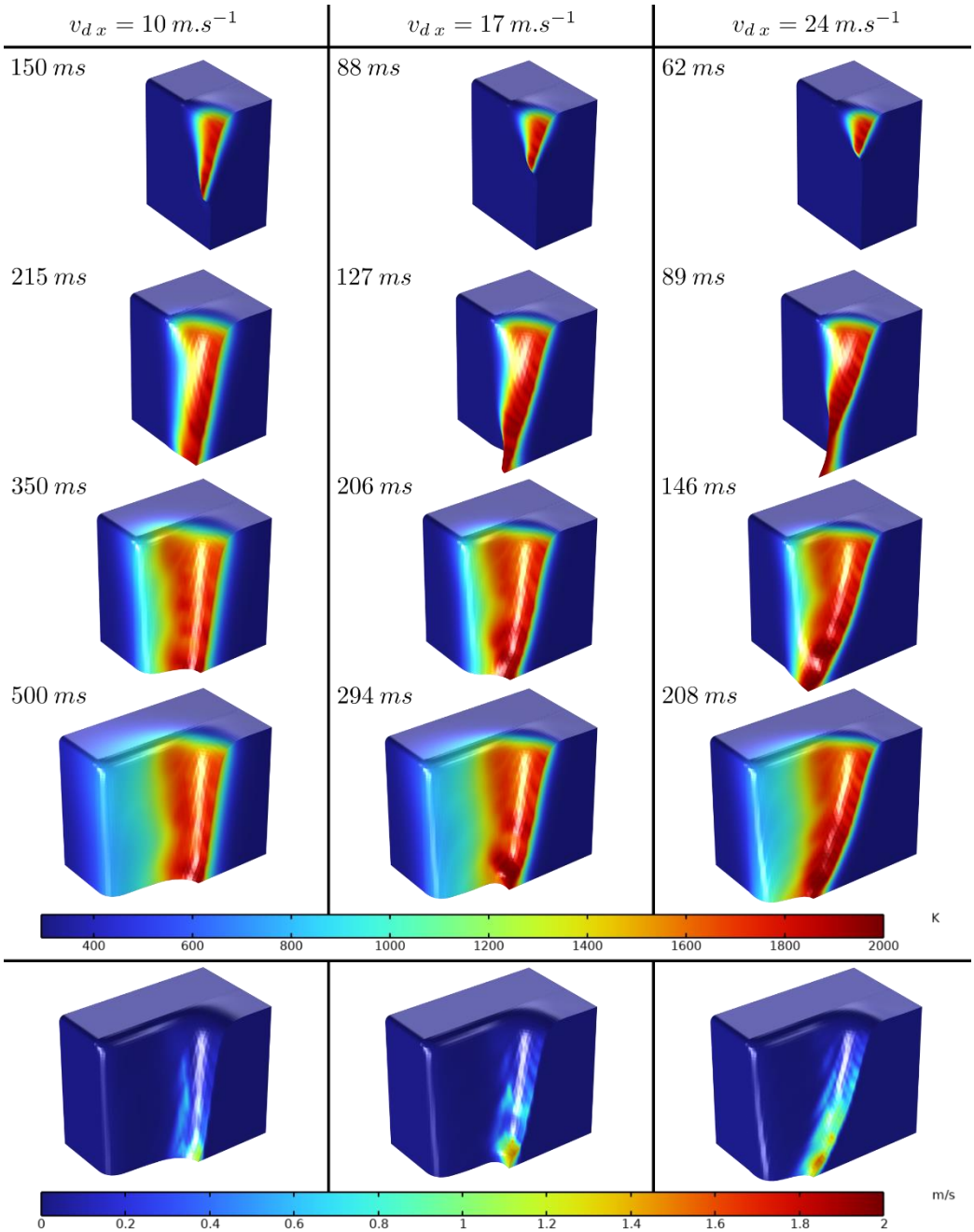

Fig. 4 Kerf shape and associated temperature and velocity magnitude fields under varying cutting velocities: **10**, **17** and **24** $\boldsymbol{m.s^{-1}}$

Fig. 5 compares the cutting front angles obtained from the experimental study [21] with those predicted by the present simulations. The results indicate a satisfying correlation, with both numerical and experimental data following a similar evolution and exhibiting only minor differences ($< 5°$). Note that the simulated cutting front angles, measured manually post-processing, may be slightly affected by the curvature of the Level Set interface on the top surface of the cutting front.

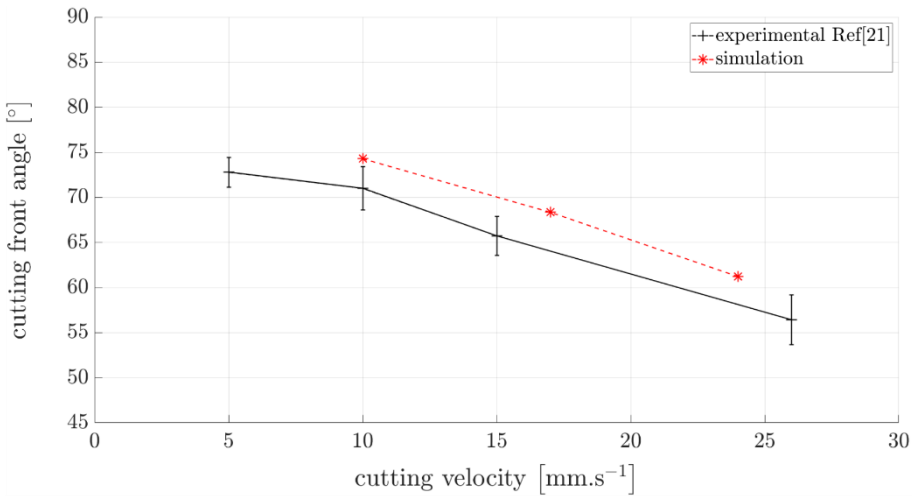

Fig. 5 Comparison between simulation and experiment of the cutting front angle $\boldsymbol{\theta}$ as a function of the cutting velocity

RESIDUAL LASER ENERGY QUANTIFICATION

Once the laser cutting process is simulated at the scale of the kerf description, the focus now relates to the quantification of the residual laser energy. Several approaches exist to model laser beam propagation, such as the electromagnetic method [32] and the ray tracing method [33]. For reasons related to feasibility, given the current computing technologies and the geometric scale, the ray tracing approach is employed.

The Level Set method is implicitly described using an Eulerian reference frame, which is incompatible with the explicit trajectory calculations of the ray tracing method. Indeed, the rays must interact with a discrete interface in order to be reflected. The objective is therefore to transform the continuous and diffuse gas-metal interface (from the Level Set method) into a discrete one. To achieve this, a moving mesh method is added to handle the interface transformation through an original dynamic coupling with the Level Set method.

The method consists of moving a mesh along the x-axis to track the iso-value $\phi = 0.5$, representing the gas-metal interface in the Level Set method, as governed by equations 22 and 23 during the laser cutting simulation. Here, $\vec{\chi}$ refers to the spatial reference system, and $\overrightarrow{u_{mm}}$

denotes the velocity of the moving mesh. Figure 6 shows the evolution of the moving mesh from time t_1 to t_5, following the gas-metal interface as defined by the thermohydrodynamic model.

$$\vec{\nabla}^2 \vec{\chi} = \overrightarrow{u_{mm}} \Delta t \tag{22}$$

$$\overrightarrow{u_{mm}} = \frac{0.5 - \phi}{0.5} \hat{x} + 0\hat{y} + 0\hat{z} \tag{23}$$

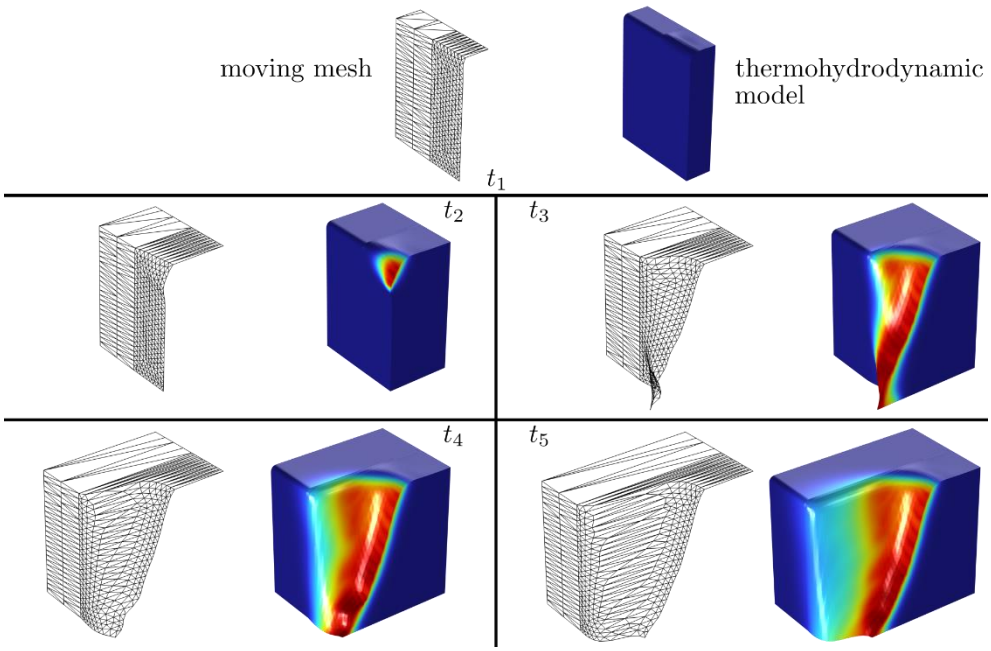

Fig. 6 Time evolution of the moving mesh method tracking the Level Set interface

After discretizing the cutting front geometry, the ray tracing method can be employed within the same simulation. As shown Fig. 6, elements are stretched, particularly along the side kerf, yet the ray tracing method remains insensitive to this deformation. Fig. 7 shows, for the same previous times (from t_1 to t_5), the ray propagation reflecting on the cutting front and reaching the background. In accordance with the experimental setup [21], rays are emitted above the laser focal plane (positioned $30\ mm$ above the plate's top surface) and converge toward the focal plane with an angle of 6°, and subsequently diverge following a Gaussian intensity profile.

Before cutting starts, at t_1 (figure 7), the background absorbs almost all of the laser beam, corresponding to nearly $4\ kW$ (or half of P_{laser}). At t_2, the cutting process begins, and the plate progressively masks a portion of the incident laser beam from reaching the background, due to interactions with the material. At t_5, when the cutting front geometry tends toward a

quasi-steady state, the residual laser energy approaches therefore a stable distribution. It should be noted that the representation of the residual laser energy on the background is dependent on its spatial discretization.

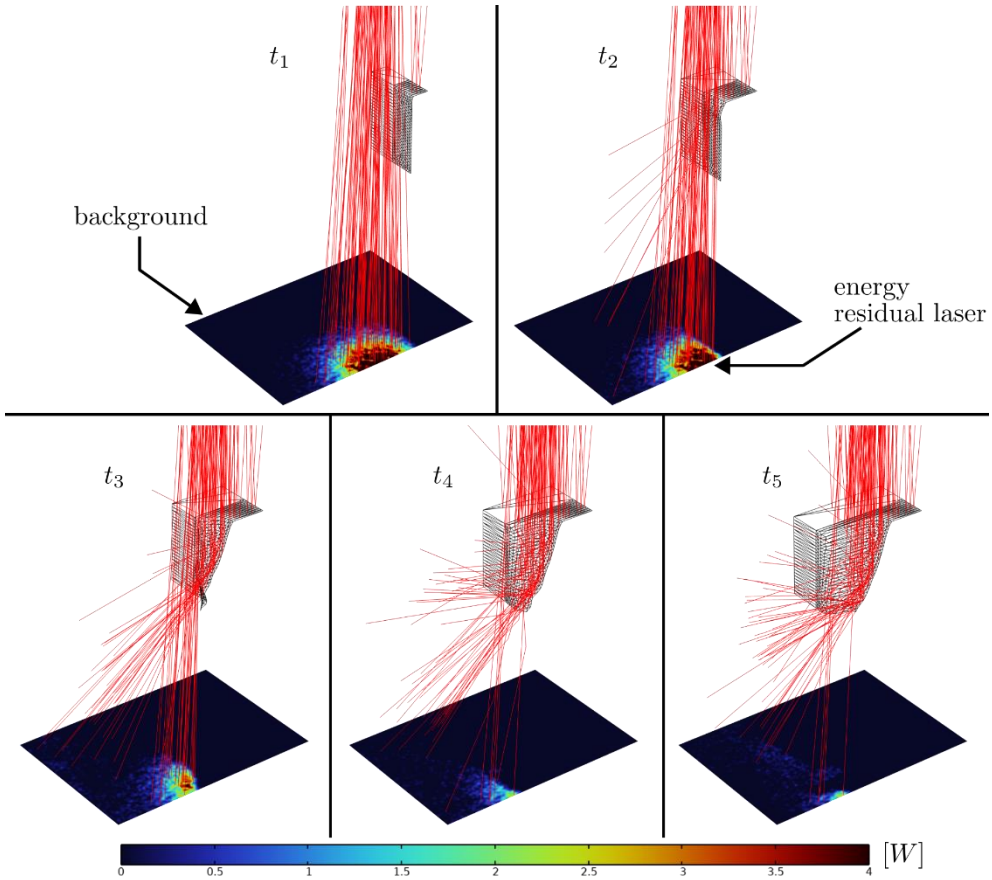

Fig. 7 Temporal evolution of ray propagation on the moving mesh

Fig. 8 presents the laser beam propagation and the residual laser energy for the three cutting velocities previously simulated using the thermohydrodynamic laser cutting model, after a plate displacement of 5 mm, corresponding to a quasi-steady state. The results indicate that as the cutting velocity increases, the residual laser energy decreases. Indeed, as previously discussed, the cutting front angle drops as the cutting velocity increases. Consequently, smaller cutting front angles result in a stronger masking effect on the laser beam reaching the background.

Rays reaching the background are classified into two groups, as also shown in Fig. 8: reflected rays and those that propagate directly to the background. Ray tracing simulations reveal that the dominant portion of the residual laser energy comes from the directly

transmitted rays, since the reflected rays are strongly diffused, and this effect becomes more pronounced with increasing background distance.

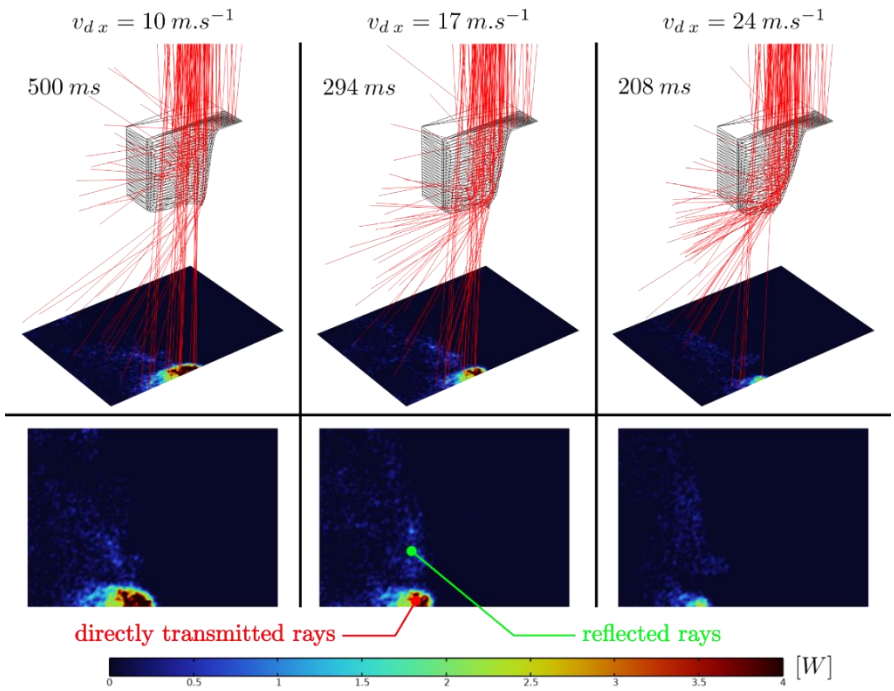

Fig. 8 Residual laser energy for the three cutting velocities

CONCLUSION

This paper introduces a thermohydrodynamic model of the laser cutting process applied to the dismantling of nuclear facilities, incorporating heat transfer, fluid flow, and gas-metal interface capturing through the Level Set method. The results demonstrate good agreement with experimental observations by comparing the cutting front angles. It is demonstrated that the model can describe the variation of the cutting front angle with respect to operating parameters, including the cutting velocity examined in this study. A hybrid Level Set – moving mesh method was then introduced to both generate a discrete gas-metal interface and enable the application of ray tracing for residual laser energy quantification. The predicted cutting front geometries is used to quantify the residual laser energy on the background, accounting for both directly transmission and reflection laser. It is shown that the reflected portion is more strongly diffused than the directly transmitted portion, and this effect should become more pronounced as the background distance from the cut plate increases.

Further work will extend the simulations to cutting in air, thereby incorporating the effects of oxidation. Additionally, simulations will be conducted on thicker plates, up to $20\,mm$, where multiple reflections of the laser at the cutting front may become significant. This effect, neglected in the literature on the thinner plates, could be more pronounced in high-thickness materials.

References

[1] A. B. J. SULIVAN and P. T. HOULDCROFT: 'Gas-jet laser cutting', *British Welding Journal*, Vol. 14, No. 8, pp. 443-445, 1967.

[2] Y. ARATA and I. MIYAMOTO: 'Generation and applications of a CW high power CO_2 gas laser', *Technology Reports Osaka University*, Vol. 17, pp. 285-290, 1967.

[3] G. PADMANABHAM and R. BATHE: 'Laser Materials Processing for Industrial Applications', *Proceedings of the National Academy of Sciences, India Section A: Physical Sciences*, Vol. 88, No. 3, pp. 359-374, somewhere, 2018.

[4] N. MUHAMMAD, D. WHITEHEAD, A. BOOR and L. LI: 'Comparison of dry and wet fibre laser profile cutting of thin 316L stainless steel tubes for medicinal device applications', *Journal of Materials Processing Technology*, Vol. 210, No. 15, pp. 2261-2267, 2010.

[5] J. LESCHKE, A. BARROI, B. EMDE, S. KAIERLE and J. HERMSDORF: 'Investigations on underwater laer cutting for decommissioning of marine constructions', *Conference on Maritime Energy (COME)*, Hamburg, Germany, 2017.

[6] K. TAMURA, R. ISHIGAMI and R. YAMAGISHI: 'Laser cutting of thick steel plates and simulated steel components using a 30 kW fiber laser', *Journal of Nuclear Science and Technology*, Vol. 53, No. 6, pp. 916-920, 2016.

[7] Y. ARATA, H. MARUO, I. MIYAMOTO and S. TAKEUCHI 'Dynamic Behavior in Laser Gas Cutting of Mild Steel', *Transactions of JWRI*, Vol. 8, No. 2, pp. 175-179, 1979.

[8] B. S. YILBAS: 'Study of Parameters for CO_2 Laser Cutting Process', *Materials and Manufacturing Processes*, Vol. 13, No. 4, pp. 517-536, 1998.

[9] C. WANDERA and V. KUJANPAA: 'Characterization of the melt removal rate in laser cutting of thick-section stainless steel', *Journal of Laser Applications*, Vol. 22, No. 2, pp. 62-70, 2010.

[10] M. SOBIH, P. L. CROUSE and L. LI: 'Elimination of striation in laser cutting of mild steel', *Journal of Physics D: Applied Physics*, Vol. 40, No. 22, pp. 6908-6916, 2007.

[11] D. SCHUÖCKER: 'Theoretical model of reactive gas-assisted laser cutting including dynamic effects', *High Power Lasers and Their Industrial Applications*, Vol. 650, No. 1, pp. 210-219, 1986.

[12] G. V. ERMOLAEV, O. B. KOVALEV, A. M. ORISHICH and V. M. FOMIN: 'Mathematical modelling of striation formation in oxygen laser cutting of mild steel', *Journal of Physics D: Applied Physics*, Vol. 39, No. 19, pp. 4236, 2006.

[13] E. H. AMARA, T. AOUDJIT, K. KHELOUFI, T. TAMSAOUT, S. AGGOUNE, A. AHMANACHE, F. HAMADI and K. BOUGHERARA: 'Simulation by temperature gradient adaption of wavelength effect in metal laser cutting', *Journal of Laser Applications*, Vol. 29, No. 2, pp. 022209, 2017.

[14] E. H. AMARA, K. KHELOUFI, T. TAMSAOUT, R. FABBRO and K. HIRANO: 'Numerical investigations on high-power laser cutting of metals', *Applied Physics A*, Vol. 119, pp. 1245-1260, 2015.

[15] K. KHELOUFI, E. H. AMARA and A. BENZAOUI: 'Numerical Simulation of Transient Three-Dimensional Temperature and Kerf Formation in Laser Fusion Cutting', *Journal of Heat and Mass Transfer*, Vol. 137, No. 11, pp. 112101, 2015.

[16] K. HIRANO and R. FABBRO: 'Experimental investigation of hydrodynamics of melt layer during laser cutting of steel', *Journal of Physics D: Applied Physics*, Vol. 44, No. 10, pp. 105502, 2011.
[17] Y. NIE, K. W. Q. LOW, Z. LIU, L. YANG, Y. WANG, T. LI, H. LI and Y. HE: 'Mechanics insights into particle ejection during laser cutting of metal alloys', *The International Journal of Advanced Manufacturing Technology*, Vol. 137, pp. 1173-1187, 2025.
[18] C. CHAGNOT, G. DE DINECHIN and G. CANNEAU: 'Cutting performances with new industrial continuous wave ND:YAG high power lasers: For dismantling of former nuclear workshops, the performances of recently introduced high power continuous wave ND:YAG lasers are addressed', *Nuclear Engineering and Design*, Vol. 240, No. 10, pp. 2604-2613, 2010.
[19] E. PORCHERON, C. DAZON, T. GELAIN, C. CHAGNOT, I. DOYEN, C. JOURNEAU, E. EXCOFFIER and D. ROULET: 'Fukushima Daiichi debris retrieval: results of aerosol characterization during laser cutting of non-radioactive corium simulants.', *Journal of Nuclear Science and Technology*, Vol. 58, No. 1, pp. 443-445, 2021.
[20] S. OSHER and J. A. SETHIAN: 'Fronts propagating with curvature-dependent speed: Algorithms based on Hamilton-Jacobi formulations', *Journal of Computational Physics*, Vol. 79, No. 1, pp. 12-49, 1988.
[21] R. MEILLOUR, M. COURTOIS, C. NAHED, M. CARIN, F. SIMON and I. DOYEN: 'Primary investigation of oxidation influence on the cutting front profile during high-thickness laser cutting', *Journal of Laser Applications*, Vol. 37, No. 2, pp. 022021, 2025.
[22] J. DUAN, H. C. MAN and T. M. YUE: 'Modelling the laser fusion cutting process: I. Mathematical modelling of the cut kerf geometry for laser fusion cutting of thick metal', *Journal of Physics D: Applied Physics*, Vol. 34, No. 14, pp. 2127-2134, 2001.
[23] M. VICANEK, G. SIMON, H. M. URBASSEK I. DECKER: 'Hydrodynamic instability of melt flow in laser cutting', *Journal of Physics D: Applied Physics*, Vol. 20, No. 1, pp. 140-145, 1987.
[24] C. LI, C. XU, C. GUI and M. D. FOX: 'Level Set evolution without re-initialization: a new variational formulation', *IEEE computer society conference on computer vision and pattern recognition*, Vol. 1, pp. 430-436, 2005.
[25] A. M. PROKHOROV: 'Laser Heating of Metals', *CRC Press*, ISBN 9781351073943, 1990.
[26] K. HIRANO, R. FABBRO and M. MULLER: 'Experimental determination of temperature threshold for melt surface deformation during laser interaction on iron at atmosphere pressure', *Journal of Physics D: Applied Physics*, Vol. 44, No. 43, pp. 435402, 2011.
[27] C. S. KIM: 'Thermophysical properties of stainless steels', *Argonne National Laboratory*, 1975.
[28] F. DAUSINGER and J. SHEN: 'Energy Coupling Efficiency in Laser Surface Treatment', *ISIJ Journal*, Vol. 33, No. 9, pp. 925-933, 1993.
[29] K. C. MILLS: *Recommended values of thermophysical properties for selected commercial alloys*, Woodhead Publishing, 2002.
[30] M. COURTOIS, M. CARIN, P. LE MASSON and S. GAIE: 'Complete 3D heat and fluid flow modeling of keyhole laser welding and methods to reduce calculation times', *Mathematical Modeling of Weld Phenomena*, Vol. 12, 2018.
[31] V. KLAPCZYNSKI, D. LE MAUX, M. COURTOIS, E. BERTRAND and P. PAILLARD: 'Surface tension measurements of liquid pure iron and 304L stainless steel under different gas misxtures', *Journal of Molecular Liquids*, Vol. 350, pp. 118558, 2022.
[32] M. COURTOIS, M. CARIN, P. LE MASSON, S. GAIED and M. BALABANE: 'A new approach to compute multi-reflections of laser beam in a keyhole for heat transfer and fluid flow modelling in laser welding', *Journal of Physics D: Applied Physics*, Vol. 46, No. 50, pp. 505305, 2013.
[33] J. DALIGAULT, M. DAL, C. GORNY, F. COSTE and R. FABBRO: 'Combination of Eulerian and ray-tracing approaches for copper laser welding simulation', *Journal of Laser Applications*, Vol. 34, No. 4, pp. 042042, 2022.